Revision 1

Interfacial structures and acidity constants of goethite from first principles molecular dynamics simulations

YINGCHUN ZHANG,[†] XIANDONG LIU,[*,†] JUN CHENG,[‡] XIANCAI LU[†]

[†]State Key Laboratory for Mineral Deposits Research, School of Earth Sciences and Engineering, Nanjing University, Nanjing, Jiangsu 210023, P. R. China

[‡]College of Chemistry and Chemical Engineering, Xiamen University, Xiamen, Fujian 361005, P. R. China

*Corresponding author: xiandongliu@gmail.com. Tel: +86 25 83594664, Fax: +86 25 83686016.

ABSTRACT

In this paper, we report a first principles molecular dynamics (FPMD) study of interfacial structures and acidity constants of goethite. The pKas of the groups on (010), (110), and (021) surfaces (in *Pbnm*) are derived with the FPMD based vertical energy gap technique. The results indicate that major reactive groups include $\equiv Fe_2OH_2$ and $\equiv FeOH_2$ on (010), $\equiv FeOH_2$, $\equiv Fe_3O_LH$, and $\equiv Fe_3O_UH$ on (110), and $\equiv FeO_hH_2$ and $\equiv Fe_2OH$ on (021). The interfacial structures were characterized in detail with a focus on the hydrogen bonding environment. With the calculated pKa values, the point of zero charges (PZCs) of the three surfaces are derived and the overall PZC range of goethite is found to be consistent with the experiment. We further discuss the potential applications of these results in future studies towards understanding the environmental processes of goethite.

Keywords: Goethite, acidity constant, interfacial structure, first principles molecular dynamics

INTRODUCTION

Goethite is the most thermodynamically stable iron oxyhydroxides at ambient temperature (Cornell and Schwertmann, 2003; Majzlan et al., 2003; Gleason et al., 2008). It is ubiquitous in soils (Sparks, 2003), lakes and marine sediments (van der Zee et al., 2003), acid mine drainage precipitates (McCarty et al., 1998; Peretyazhko et al., 2009), and on Mars (Klingelhoefer et al., 2005). Goethite usually expresses acicular habit and is enclosed by (110), (010), and (021) surfaces (Cornell and Schwertmann, 2003). Due to its high specific surface area (up to 200 m^2/g) (Schwertmann and Taylor, 1989) and reactivity (Schwertmann and Cornell, 2000), goethite has a profound effect on the retention of heavy metals cations and negatively-charged moieties (e.g., As/P oxyanions and organic acids) (Fendorf et al., 1997; Randall et al., 1999; Filius et al., 2000; Ostergren et al., 2000; Kaiser and Guggenberger, 2007).

Due to the presence of amphoteric surface groups (i.e. OH/OH_2 of singly, doubly, and triply coordinated Fe sites), goethite surfaces can both donate and accept protons, and the interfacial properties including complexing of cations and anions are pH-dependent. For example, the adsorption capacities of heavy metal cations and oxyanions increase and decrease with pH, respectively (Grossl et al., 1997; Kim et al., 2011; Mamindy-Pajany et al., 2011; Komárek et al., 2018). It was also found that As/P oxyanions and carboxylate groups can form bidentate complexes at low pH and monodentate or hydrogen-bonded outer-sphere complexes at high pH (Fendorf et al., 1997; Manning et al., 1998; Filius et al., 2000; Ona-Nguema et al., 2005; Persson and

Axe, 2005; Hanna et al., 2014; Marsac et al., 2016; Yang et al., 2016; Yan and Jing, 2018). As common heavy metal contaminants in water and soils, Pb(II) and Cd(II) were selected as model cations in many experimental and modeling studies (Spadini et al., 1994; Venema et al., 1997; Randall et al., 1999; Ostergren et al., 2000; Elzinga et al., 2001; Boily et al., 2005; Granados-Correa et al., 2011; Leung and Criscenti, 2017; Liu et al., 2018). Using extended x-ray absorption fine structure (EXAFS) spectroscopy, it was found that Pb(II) and Cd(II) form predominantly edge-sharing and corner-sharing complexes on goethite, respectively (Randall et al., 1999; Ostergren et al., 2000). Despite the extensive studies, the microscopic complexation mechanisms of heavy metal cations, including the complexing sites and structures on different facets and the corresponding pH-dependence were still poorly understood.

The identities and intrinsic acidity constants of surface groups on goethite are central to the understanding of the pH-dependent interfacial processes. Unfortunately, current experimental techniques are unable to distinguish the pKas of minerals with so many facets and surface sites. Several theoretical approaches including MUSIC method, static density functional theory (DFT) calculations, and first-principles molecular dynamics (FPMD) simulations have been utilized to calculate the pKas of goethite. MUSIC method (Hiemstra et al., 1989) correlates the surface pKa with the undersaturation of surface oxygen based on bond valence and it is able to calculate the acidities of groups on different surfaces (Hiemstra et al., 1996). With this method, the pKas of the groups on (110), (021), and (100) surfaces were obtained, and the corresponding point of zero charge (PZC) matched with the measured values

(Venema et al., 1998; Gaboriaud and Ehrhardt, 2003). Despite this agreement, the pKas cannot be uniquely determined using MUSIC method. For example, essentially different pKas were obtained for several groups when hydrogen bond contributions and Fe-O distances derived from classical molecular dynamics simulations were used as the input of MUSIC (Boily, 2012). According to previous studies, the pKa values predicted by MUSIC with different proton bond valences and hydrogen bonding environments can vary up to 5 and 8 pKa units, respectively (Boily et al., 2001; Gaboriaud and Ehrhardt, 2003). Aquino et al. (2008) derived pKa values based on the deprotonation free energies from static DFT calculations with cluster surface models and simplified continuum solvent models. However, the cluster models cannot distinguish the pKas of different surfaces.

In recent years, FPMD method with periodic surface model and explicit solvent have been applied to calculate the free energies for a variety of chemical processes at mineral-water interfaces (Boulet et al., 2006; Watts et al., 2014; Churakov, 2015; Gaigeot and Sulpizi, 2016; Pouvreau et al., 2017; Churakov and Liu, 2018; Gaigeot and Sulpizi, 2020). For example, by employing FPMD based free energy calculations, Klyukin et al. (2018) investigated the release of iron from goethite (110) and (021) facets. Leung and Criscenti (2012) calculated the potential of mean force associated with the deprotonation of $\equiv FeOH_2$ on (110) surface and obtained a pKa of 7.0. However, to our knowledge, a dataset of pKas at the FPMD level is still lacking for goethite surfaces.

FPMD based vertical energy gap method developed by Sprik group at Cambridge has proven powerful in pKa prediction (Sulpizi and Sprik, 2008; Costanzo et al., 2011). This method has been validated on molecular acids spanning over 20 pKa units with an accuracy of 2 pKa units (Park et al., 2006; Cheng et al., 2009; Sulpizi and Sprik, 2010; Costanzo et al., 2011; Mangold et al., 2011; Cheng et al., 2014). It has been successfully applied to derive the pKas of surface groups of oxides (Cheng and Sprik, 2010; Gaigeot et al., 2012; Sulpizi et al., 2012; Liu et al., 2014a; Gittus et al., 2018), hydroxides (Liu et al., 2013a) and clay minerals (Liu et al., 2013b; Liu et al., 2014b). In the present study, this technique was applied to calculate the pKas of major surfaces of goethite (i.e. (010), (110), and (021)). The interfacial structures are characterized in detail and the reactive groups have been identified based on the calculated pKas.

COMPUTATIONAL METHODS

The models

The crystal parameters of goethite used to build surface models are a=4.616 Å,b= 9.956 Å, c=3.025 Å and $\alpha=\beta=\gamma=90°$ (in *Pbnm*) (Alvarez et al., 2008). The (010) surface (Figure 1a) consisted of 2×1×3 unit cells and it was cut from the bulk crystal based on the structure from crystal truncation rod analysis (Ghose et al., 2010). Singly and doubly coordinated groups exist on this surface (i.e. $\equiv FeOH_2$ and $\equiv Fe_2OH$). (110) and (021) surfaces were cleaved from the bulk crystal according to the structures available in the literature (Aquino et al., 2007; Rustad and Boily, 2010; Boily, 2012; Kubicki et al., 2012; Leung and Criscenti, 2012; Alexandrov and Rosso, 2015;

Kubicki et al., 2017). One singly coordinated group (≡FeOH), one doubly coordinated group (≡Fe_2OH), and three triply coordinated groups (lower site: ≡Fe_3O_LH; upper site: ≡Fe_3O_UH; site without proton: ≡Fe_3O) are present on (110) surface (Figure 1b). On (021) surface (Figure 1c), there are two kinds of singly coordinated groups (≡FeO_hH_2 coordinated with water and ≡FeOH coordinated with OH) and two doubly coordinated groups (≡Fe_2OH at structural O site and ≡Fe_2O_hH at structural OH site). All of the surface models created in the present study bear no net charge.

The surface models were placed in 3D periodically repeated orthorhombic cells with a solution region of 16 Å. The dimensions of the simulation cells are 9.074×9.233×28.000 $Å^3$ for (010) system, 9.074×10.975×26.000 $Å^3$ for (110) system, and 9.233×11.650×26.000 $Å^3$ for (021) system. 45, 53, and 58 water molecules were randomly placed in the solution regions of (010), (110), and (021) systems respectively. These numbers were determined from the density of bulk water. The water density profiles derived from the trajectories (Figure S1 in the Supplemental[1] material) suggested that the ambient water density was reached in the bulk regions.

FPMD Details

The CP2K/QUICKSTEP package (VandeVondele et al., 2005; Hutter et al., 2014) was used to conduct all FPMD simulations. In this package, the electronic structures were calculated with the hybrid Gaussian and Plane Wave (GPW) approach (Lippert et al., 1997). A double-ζ Gaussian-type orbital basis (VandeVondele and Hutter, 2007) with polarization functions (DZVP) was employed to construct the electronic wavefunctions. The plane wave basis was expanded to 360 Ry to represent the

electron density. The Goedecker-Teter-Hutter (GTH) pseudopotentials (Goedecker et al., 1995) were used to represent the core electrons states. The Perdew–Burke–Ernzerhof (PBE) functional (Perdew et al., 1997) was used to describe the exchange-correlation interaction. Van der Waals interactions were taken into account by using the DFT-D3 dispersion corrections (Grimme et al., 2010). Wave functions were optimized to a tolerance of 1.0E-6.

All calculations were spin-polarized with the spin multiplicity set to unity. Antiferromagnetic ordering was adopted as the initial spin configurations for all the systems with up/down spin Fe atoms locating at alternating layers along [010] direction (Kubicki et al., 2008; Martin et al., 2009; Kerisit et al., 2016; Bylaska et al., 2020) (Figure 1). The antiferromagnetic configuration was maintained during the simulations. Our calculations predicted a pKa of 7.3 for $\equiv FeOH_2$ on (110) surface, which is consistent with 7.0 obtained by Leung and Criscenti (2012) using DFT+U based FPMD simulation. This agreement indicates that the Hubbard U correction does not have obvious influence on the pKa estimate for the current systems.

Born-Oppenheimer type molecular dynamics (BOMD) simulations were carried out with a time step of 0.5 fs. NVT ensemble with the Nosé-Hoover chain thermostat was adopted to propagate the simulations. The temperature was controlled at 330 K. This temperature was intended to avoid the glassy behavior of liquid water at a lower temperature (VandeVondele et al., 2004). For each FPMD simulation, an equilibration runs for at least 2.0 ps was conducted, followed by a production run for over 10.0 ps.

The pKa values of goethite surface groups were evaluated with the half-reaction scheme of the vertical energy gap method (Sulpizi and Sprik, 2008; Cheng et al., 2009; Costanzo et al., 2011; Cheng and Sprik, 2012). With this method, the free energy change of the deprotonation reaction is calculated as the integral of the ensemble averages of the vertical energy gaps obtained from a series of FPMD trajectories along the alchemical path from reactant state to product state. The details are given in section S2 in the Supplemental[1] material.

RESULTS AND DISCUSSION

Interfacial structures and pKas

(010) surface. During the free MD simulation, two H_2O ligands out of 12 $\equiv FeOH_2$ groups left from the Fe atoms, indicating a weak interaction between Fe and the coordinated water. Similar detachment was also observed in the FPMD study of Chen et al. (2017). $\equiv FeOH_2$ can donate hydrogen bonds to solvent water and the average coordination number (CN) of water O around the H of $\equiv FeOH_2$ is 0.5 (Figure 3a). $\equiv Fe_2OH$ donates a hydrogen bond to $\equiv Fe_3O$ in the bulk and at the same time it accepts on average 0.7 hydrogen bonds from the solvent water (Figure 3b).

The calculated energy gaps and deprotonation free energies of (010) surface groups are listed in Supplemental[1] Table S2, and the obtained pKas are summarized in Table 1. It can be seen that the vertical energy gaps converge within 0.26 eV (Supplemental[1] Table S2) and the calculated pKas have statistical errors within 2.0 pKa units (Tables 1-3). The calculated pKa of $\equiv FeOH_2$ is 10.9, indicating that this group remains protonated in the near neutral pH range and the deprotonated form can

occur under basic conditions. The pKas of ≡Fe_2OH and ≡Fe_2OH_2 are 15.4 and 4.7, respectively, implying that ≡Fe_2OH is the most possible form, whereas ≡Fe_2OH_2 mainly occurs in acidic pH range. Using hydrogen bond valence derived from classical molecular dynamics simulations, MUSIC method predicted a pKa of 4.3 for ≡Fe_2OH_2, which is consistent with our prediction (Boily, 2012). No MUSIC result was reported for ≡Fe_2OH to the best of our knowledge.

(110) surface. Most of the OHs of ≡FeOH sites show orientations parallel to the surface and the rest pointed towards the solution region (Figure 4). Therefore, the parallelly orientated ≡FeOH can accept hydrogen bonds from both ≡Fe_3O_LH groups and solvent water while the others donate hydrogen bonds to solvent water (Figure 4). The different orientations of OHs were also observed on other (hydr)oxides surfaces, e.g., gibbsite (Liu et al., 2013a), corundum (Gaigeot et al., 2012), and hematite (von Rudorff et al., 2016). The OHs of ≡FeOH can switch between the two orientations and the overall CN between water H and the O of ≡FeOH is 0.97 (Figure 5a). The OHs of ≡Fe_2OH and ≡Fe_3O_UH point towards the solution region, and both donate hydrogen bonds to solvent water, with an average CN of 0.97 (Figure 6b) and 0.85 (Figure 5b) respectively. ≡Fe_2OH also accepts one hydrogen bond from solvent water (Figure 6a). ≡Fe_3O has no contact with water because of the steric hindrance (Figure 5c).

The pKas of ≡FeOH and ≡$FeOH_2$ are 15.0 and 7.3 respectively (Table 2). Although the computed pKa of ≡FeOH is smaller than the MUSIC prediction 19.6 (Venema et al., 1998), they both indicate that ≡FeOH is inert. The pKa of ≡$FeOH_2$ is

similar to the previous FPMD result 7.0 (Leung and Criscenti, 2012) and the MUSIC result 7.7 (Venema et al., 1998). However, the MUSIC prediction for these groups will be significantly different if a different hydrogen bonding environment was used (11.7 or 3.7 and 23.6 or 15.6 would be obtained for ≡$FeOH_2$ and ≡FeOH when it was assumed that 1 or 3 hydrogen bonds were formed with water) (Gaboriaud and Ehrhardt, 2003). Nevertheless, the calculated pKas suggest that ≡FeOH can get protonated and therefore both ≡FeOH and ≡$FeOH_2$ can exist in normal pH range.

≡Fe_2OH and ≡Fe_2OH_2 have pKas of 13.9 and -0.5, respectively, which are close to the MUSIC predictions 12.3 and 0.4 (Venema et al., 1998). Such a low acidity constant for ≡Fe_2OH_2 indicates that ≡Fe_2OH hardly accepts a second proton at common pH.

The pKa values of ≡Fe_3O_LH, ≡Fe_3O_UH, and≡Fe_3OH are calculated to be 10.7, 9.7, and 0.3, respectively. MUSIC method cannot discriminate ≡Fe_3O_LH and ≡Fe_3O_UH and gave a pKa of 11.7 (Venema et al., 1998). This value agrees with the pKas obtained for ≡Fe_3O_LH and ≡Fe_3O_UH. However, this should be considered fortuitous as the hydrogen bonding environments are different for these two groups: ≡Fe_3O_LH forms a hydrogen bond with ≡FeOH while ≡Fe_3O_UH donates a hydrogen bond to water. For ≡Fe_3OH, the MUSIC result was -0.2 (Venema et al., 1998), close to our prediction. Overall, the calculated pKas indicate that ≡Fe_3O_LH and ≡Fe_3O_UH are stable in common pH.

(021) surface. On (021) surface, the coordinated H_2O of ≡FeO_hH_2 sites are loosely bound and can leave the surface spontaneously during the free MD simulation. This

observation is consistent with the low desorption energy of ~0.5 kcal/mol for H_2O on this site (Alexandrov and Rosso, 2015). $\equiv FeO_hH_2$ accepts hydrogen bonds from solvent water with a CN of 0.3 (Figures 7a and 8a). The two OHs of $\equiv FeO_hH_2$ also donate hydrogen bonds to the nearby $\equiv FeOH$ and $\equiv Fe_2OH$ groups (Figure 7b). $\equiv FeOH$ can donate and accept hydrogen bonds to/from solvent water, with a CN of 0.7 and 0.3, respectively (Figures 7a and 9). $\equiv Fe_2OH$ and $\equiv Fe_2O_hH$ donate hydrogen bonds to $\equiv FeOH$ (Figure 7b). $\equiv Fe_2OH$ also donates hydrogen bonds to solvent water with a CN of 0.3 (Figure 8b), while $\equiv Fe_2O_hH$ accepts hydrogen bonds from solvent water with a CN of 0.4 (Figure 8c). Overall, the interaction between the first layer water and surface groups on (021) surface is weaker compared to those on (010) and (110) surfaces, as revealed by the smaller CNs between surface groups and water.

The calculated pKa of $\equiv FeO_hH_2$ is 10.0 (Table 3), close to the MUSIC result 11.9 (Venema et al., 1998). $\equiv FeOH$ and $\equiv FeOH_2$ have pKas of 12.2 and 2.3, respectively, indicating that $\equiv FeOH_2$ rarely happens and $\equiv FeOH$ is the most possible form in common pH range. MUSIC results were 20.0 and 8.1 for $\equiv FeOH$ and $\equiv FeOH_2$, respectively (Venema et al., 1998), which are substantially higher than our results.

The calculated pKas for $\equiv Fe_2O_hH/\equiv Fe_2O_hH_2$ and $\equiv Fe_2OH/\equiv Fe_2OH_2$ are 13.2/0.8 and 5.2/-1.3, respectively. The higher pKa value of $\equiv Fe_2O_hH$ compared to $\equiv Fe_2OH$ is consistent with the different roles they played in hydrogen bonding, that is, $\equiv Fe_2O_hH$ was proton acceptor while $\equiv Fe_2OH$ was proton donor. MUSIC predictions were 19.6/7.7 for $\equiv Fe_2O_hH/\equiv Fe_2O_hH_2$ and 11.9/0.0 for $\equiv Fe_2OH/\equiv Fe_2OH_2$ (Venema et al., 1998). Although these values were different from our results, the MUSIC predictions

also demonstrated a decreasing trend from $\equiv Fe_2O_hH$ to $\equiv Fe_2OH$. Overall, our calculated pKas suggest that the protonated $\equiv Fe_2O_hH_2$ and $\equiv Fe_2OH_2$ rarely occur; $\equiv Fe_2O_hH$ is inactive in normal pH range and $\equiv Fe_2OH$ can get deprotonated in slightly acidic conditions.

Surface charging

PZC is an important parameter in surface complexation reactions because it determines the sign of surface charges at a certain pH. PZC of a certain surface can be estimated based on the surface pKas (Table 4). For the (010) surface, the PZC is estimated to be 7.8, which is determined by the pKas of $\equiv FeOH_2$ and $\equiv Fe_2OH_2$. Similarly, the PZCs of (110) and (021) are 8.5 and 3.8, respectively. Therefore, the PZC of a whole goethite should be in the range of 3.8~8.5, which is consistent with the experimental range of 5.6~9.5 (Lutzenkirchen, 2002; Lützenkirchen et al., 2008; Kosmulski, 2009). The PZC values of (010) and (110) surfaces are very close, and they are significantly higher than the PZC of (021) surface.

At pH below 3.8 (i.e. PZC of (021) surface), all three surfaces are positively charged and therefore adsorption of heavy metal cations is inhibited. This is consistent with the fact that heavy metals do not show adsorption (e.g. Cd, Zn) or only marginal adsorption (e.g. Pb, Cu) on goethite at pH below 3.8 (Komárek et al., 2018). As pH increases, the net charges on (010) and (110) surfaces decrease and they bear net negative charges at pH above 7.8 and 8.5, respectively. These values are in general coincidence with the pH range where the adsorption capacity reached the maximum (Komárek et al., 2018).

IMPLICATIONS

Based on the computed pKas, the surface sites available for complexing metal cations can be derived and they include ≡FeOH on (010) surface, ≡FeOH, ≡Fe_3O_L, and ≡Fe_3O_U on (110) surface, and ≡Fe_2O, ≡FeOH, and ≡FeO_hH on (021) surface. The complexation mechanisms of heavy metals at a certain pH can be deduced based on the distributions of available complexing sites. As an example, the distance between two neighboring ≡FeOH groups on (110) surface is ~3.0 Å, and therefore a bidentate corner-sharing complex can form on these sites in near-neutral conditions (Randall et al., 1999). The relative stabilities of the complexes on different sites can be obtained by comparing FPMD calculated free energies. For example, with such an approach we investigated the thermodynamics of Cd(II) and Ni(II) complexes formed on clay edge sites (Zhang et al., 2016; Zhang et al., 2017).

There is a consensus that anionic groups (e.g. soil organic matters (SOMs), As/P oxyanions) can form inner-sphere complexes on goethite via ligand exchange reactions (Gu et al., 1994; Grossl et al., 1997; Kaiser et al., 1997; Kaiser et al., 2007; Kim et al., 2011). pH dependence of complexation of anionic groups can be derived by integrating surface pKas and FPMD computed adsorption free energies, e.g. with this approach we investigated the complexation mechanisms of acetate, quinone, and phosphate on clay edges as a function of pH (Liu et al., 2017; Lützenkirchen et al., 2018; Zhang et al., 2020).

The pKas calculated in the present study are of high accuracy and can be directly applied with SCMs (Nie et al., 2017; Han and Katz, 2019) to investigate the

adsorption behaviors. For example, based on the surface sites and pKas derived in our prior studies (Liu et al., 2012a; Liu et al., 2012b; Liu et al., 2013b; Liu et al., 2014b). Tournassat et al. developed a SCM for clay edges, that successfully reproduced the experimental acid-base titration data of montmorillonite (Tournassat et al., 2016) and the adsorption of uranyl over a wide range of pH and concentration conditions (Tournassat et al., 2018; Zhang et al., 2018). The integration of the computed intrinsic pKas into the SCM modeling can establish direct links between macroscopic experiments and microscopic properties, that can thus help uncover the adsorption mechanisms. Overall, the structures and pKas obtained in the present study form a microscopic basis for understanding the environmental and geochemical processes at goethite interfaces.

304

305 ## ACKNOWLEDGMENTS AND FUNDING

306 This study was supported by the National Natural Science Foundation of China
307 (No. 41872041 and 41572027). We acknowledge the financial support from the State
308 Key Laboratory for Mineral Deposits Research at Nanjing University. We are grateful
309 to the High Performance Computing Center (HPCC) of Nanjing University for doing
310 the numerical calculations in this paper on its blade cluster system.

311

312

313 **REFERENCES CITED**

314 Alexandrov, V., and Rosso, K.M. (2015) Ab initio modeling of Fe(II) adsorption and
315 interfacial electron transfer at goethite (α-FeOOH) surfaces. Physical Chemistry
316 Chemical Physics, 17, 14518-14531.
317 Alvarez, M., Sileo, E.E., and Rueda, E.H. (2008) Structure and reactivity of synthetic
318 co-substituted goethites. American Mineralogist, 93, 584-590.
319 Aquino, A.J.A., Tunega, D., Haberhauer, G., Gerzabek, M.H., and Lischka, H. (2007)
320 Quantum chemical adsorption studies on the (110) surface of the mineral goethite.
321 The Journal of Physical Chemistry C, 111, 877-885.
322 Aquino, A.J.A., Tunega, D., Haberhauer, G., Gerzabek, M.H., and Lischka, H. (2008)
323 Acid–base properties of a goethite surface model: A theoretical view. Geochimica
324 et Cosmochimica Acta, 72, 3587-3602.
325 Boily, J.-F. (2012) Water structure and hydrogen bonding at goethite/water interfaces:
326 Implications for proton affinities. The Journal of Physical Chemistry C, 116,
327 4714-4724.
328 Boily, J.-F., Lützenkirchen, J., Balmès, O., Beattie, J., and Sjöberg, S. (2001)
329 Modeling proton binding at the goethite (α-FeOOH)–water interface. Colloids and
330 Surfaces A: Physicochemical and Engineering Aspects, 179, 11-27.
331 Boily, J.-F., Sjöberg, S., and Persson, P. (2005) Structures and stabilities of Cd(II) and
332 Cd(II)-phthalate complexes at the goethite/water interface. Geochimica et
333 Cosmochimica Acta, 69, 3219-3235.
334 Boulet, P., Greenwell, H.C., Stackhouse, S., and Coveney, P.V. (2006) Recent
335 advances in understanding the structure and reactivity of clays using electronic
336 structure calculations. Journal of Molecular Structure: THEOCHEM, 762, 33-48.
337 Bylaska, E.J., Song, D., and Rosso, K.M. (2020) Electron transfer calculations
338 between edge sharing octahedra in hematite, goethite, and annite. Geochimica et
339 Cosmochimica Acta, 291, 79-91.Chen, Y., Bylaska, E.J., and Weare, J.H. (2017)
340 Weakly bound water structure, bond valence saturation and water dynamics at the
341 goethite (100) surface/aqueous interface: Ab initio dynamical simulations.
342 Geochemical Transactions, 18, 3.
343 Cheng, J., Liu, X., VandeVondele, J., Sulpizi, M., and Sprik, M. (2014) Redox
344 potentials and acidity constants from density functional theory based molecular
345 dynamics. Accounts of Chemical Research, 47, 3522-3529.
346 Cheng, J., and Sprik, M. (2010) Acidity of the aqueous rutile TiO2(110) surface from
347 density functional theory based molecular dynamics. Journal of Chemical Theory
348 and Computation, 6, 880-889.
349 Cheng, J., and Sprik, M. (2012) Alignment of electronic energy levels at
350 electrochemical interfaces. Physical Chemistry Chemical Physics, 14,
351 11245-11267.
352 Cheng, J., Sulpizi, M., and Sprik, M. (2009) Redox potentials and pk(a) for
353 benzoquinone from density functional theory based molecular dynamics. Journal

of Chemical Physics, 131, 154504.
Churakov, S.V. (2015) Ab initio simulations of mineral surfaces: Recent advances in numerical methods and selected applications. In Armbruster, T., Danisi, R.M. Eds., Highlights in mineralogical crystallography, pp. 75-108. De Gruyter, Berlin, Boston.
Churakov, S.V., and Liu, X. (2018) Quantum-chemical modelling of clay mineral surfaces and clay mineral–surface–adsorbate interactions. In Schoonheydt, R., Johnston, C.T., Bergaya, F. Eds., Developments in clay science, pp. 49-87. Elsevier.
Cornell, R.M., and Schwertmann, U. (2003) The iron oxides: Structure, properties, reactions, occurrences and uses. John Wiley & Sons.
Costanzo, F., Sulpizi, M., Valle, R.G.D., and Sprik, M. (2011) The oxidation of tyrosine and tryptophan studied by a molecular dynamics normal hydrogen electrode. The Journal of Chemical Physics, 134, 244508.
Elzinga, E.J., Peak, D., and Sparks, D.L. (2001) Spectroscopic studies of Pb(II)-sulfate interactions at the goethite-water interface. Geochimica et Cosmochimica Acta, 65, 2219-2230.
Fendorf, S., Eick, M.J., Grossl, P., and Sparks, D.L. (1997) Arsenate and chromate retention mechanisms on goethite. 1. Surface structure. Environmental Science & Technology, 31, 315-320.
Filius, J.D., Lumsdon, D.G., Meeussen, J.C.L., Hiemstra, T., and Van Riemsdijk, W.H. (2000) Adsorption of fulvic acid on goethite. Geochimica et Cosmochimica Acta, 64, 51-60.
Gaboriaud, F., and Ehrhardt, J.-J. (2003) Effects of different crystal faces on the surface charge of colloidal goethite (α-FeOOH) particles: An experimental and modeling study. Geochimica et Cosmochimica Acta, 67, 967-983.
Gaigeot, M.-P., and Sulpizi, M. (2016) Mineral–water interaction. In Kubicki, J.D. Ed., Molecular modeling of geochemical reactions, pp. 271-309. Wiley, Hoboken.
Gaigeot, M.-P., and Sulpizi, M. (2020) Structure and dynamics of solid/liquid interfaces. In Wandelt, K. Ed., Surface and interface science, pp. 143-196. Wiley, Hoboken.
Gaigeot, M.P., Sprik, M., and Sulpizi, M. (2012) Oxide/water interfaces: How the surface chemistry modifies interfacial water properties. Journal of Physics: Condensed Matter, 24, 124106-124116.
Ghose, S.K., Waychunas, G.A., Trainor, T.P., and Eng, P.J. (2010) Hydrated goethite (α-FeOOH) (100) interface structure: Ordered water and surface functional groups. Geochimica et Cosmochimica Acta, 74, 1943-1953.
Gittus, O.R., von Rudorff, G.F., Rosso, K.M., and Blumberger, J. (2018) Acidity constants of the hematite–liquid water interface from ab initio molecular dynamics. The Journal of Physical Chemistry Letters, 9, 5574-5582.
Gleason, A.E., Jeanloz, R., and Kunz, M. (2008) Pressure-temperature stability studies of feooh using X-ray diffraction. American Mineralogist, 93, 1882-1885.
Goedecker, S., Teter, M., and Hutter, J. (1995) Separable dual-space gaussian pseudopotentials. Physical Review B Condensed Matter, 54, 1703-1710.

Granados-Correa, F., Corral-Capulin, N.G., Olguín, M.T., and Acosta-León, C.E. (2011) Comparison of the Cd(II) adsorption processes between boehmite (γ-AlOOH) and goethite (α-FeOOH). Chemical Engineering Journal, 171, 1027-1034.

Grimme, S., Antony, J., Ehrlich, S., and Krieg, H. (2010) A consistent and accurate ab initio parametrization of density functional dispersion correction (DFT-D) for the 94 elements H-Pu. Journal of Chemical Physics, 132, 154104.

Grossl, P.R., Eick, M., Sparks, D.L., Goldberg, S., and Ainsworth, C.C. (1997) Arsenate and chromate retention mechanisms on goethite. 2. Kinetic evaluation using a pressure-jump relaxation technique. Environmental Science & Technology, 31, 321-326.

Gu, B., Schmitt, J., Chen, Z., Liang, L., and McCarthy, J.F. (1994) Adsorption and desorption of natural organic matter on iron oxide: Mechanisms and models. Environmental Science & Technology, 28, 38-46.

Han, J., and Katz, L.E. (2019) Capturing the variable reactivity of goethites in surface complexation modeling by correlating model parameters with specific surface area. Geochimica et Cosmochimica Acta, 244, 248-263.

Hanna, K., Martin, S., Quilès, F., and Boily, J.F. (2014) Sorption of phthalic acid at goethite surfaces under flow-through conditions. Langmuir, 30, 6800-6807.

Hiemstra, T., Riemsdijk, W.H.V., and Bolt, G.H. (1989) Multisite proton adsorption modeling at the solid/solution interface of (hydr)oxides: A new approach. I. Model description and evaluation of intrinsic constants. Journal of Colloid and Interface Science, 133, 91-104.

Hiemstra, T., Venema, P., and Riemsdijk, W.H.V. (1996) Intrinsic proton affinity of reactive surface groups of metal (hydr)oxides: The bond valence principle. Journal of Colloid and Interface Science, 184, 680-692.

Hutter, J., Iannuzzi, M., Schiffmann, F., and VandeVondele, J. (2014) CP2K: Atomistic simulations of condensed matter systems. Wiley Interdisciplinary Reviews: Computational Molecular Science, 4, 15-25.

Kaiser, K., and Guggenberger, G. (2007) Sorptive stabilization of organic matter by microporous goethite: Sorption into small pores vs. Surface complexation. European Journal of Soil Science, 58, 45-59.

Kaiser, K., Guggenberger, G., Haumaier, L., and Zech, W. (1997) Dissolved organic matter sorption on sub soils and minerals studied by 13C-NMR and DRIFT spectroscopy. European Journal of Soil Science, 48, 301-310.

Kaiser, K., Mikutta, R., and Guggenberger, G. (2007) Increased stability of organic matter sorbed to ferrihydrite and goethite on aging. Soil Science Society of America Journal, 71, 711-719.

Kerisit, S., Bylaska, E.J., Massey, M.S., McBriarty, M.E., and Ilton, E.S. (2016) Ab initio molecular dynamics of uranium incorporated in goethite (α-FeOOH): Interpretation of X-ray absorption spectroscopy of trace polyvalent metals. Inorganic Chemistry, 55, 11736-11746.

Kim, J., Li, W., Philips, B.L., and Grey, C.P. (2011) Phosphate adsorption on the iron oxyhydroxides goethite (α-FeOOH), akaganeite (β-FeOOH), and lepidocrocite

(γ-FeOOH): A 31P NMR study. Energy & Environmental Science, 4, 4298-4305.

Klingelhoefer, G., DeGrave, E., Morris, R.V., Van Alboom, A., De Resende, V., De Souza, P., Rodionov, D., Schröder, C., Ming, D., and Yen, A. (2005) Mössbauer spectroscopy on mars: Goethite in the columbia hills at gusev crater. Hyperfine Interactions, 166, 549-554.

Klyukin, K., Rosso, K.M., and Alexandrov, V. (2018) Iron dissolution from goethite (α-FeOOH) surfaces in water by ab initio enhanced free-energy simulations. The Journal of Physical Chemistry C, 122, 16086-16091.

Komárek, M., Antelo, J., Králová, M., Veselská, V., Číhalová, S., Chrastný, V., Ettler, V., Filip, J., Yu, Q., Fein, J.B., and Koretsky, C.M. (2018) Revisiting models of Cd, Cu, Pb and Zn adsorption onto Fe(III) oxides. Chemical Geology, 493, 189-198.

Kosmulski, M. (2009) Surface charging and points of zero charge, Surfactant science Series, vol. 145. CRC press, Boca Raton, Florida.

Kubicki, J.D., Paul, K.W., Kabalan, L., Zhu, Q., Mrozik, M.K., Aryanpour, M., Pierre-Louis, A.-M., and Strongin, D.R. (2012) ATR–FTIR and density functional theory study of the structures, energetics, and vibrational spectra of phosphate adsorbed onto goethite. Langmuir, 28, 14573-14587.

Kubicki, J.D., Paul, K.W., and Sparks, D.L. (2008) Periodic density functional theory calculations of bulk and the (010) surface of goethite. Geochemical Transactions, 9, 4.

Kubicki, J.D., Tunega, D., and Kraemer, S. (2017) A density functional theory investigation of oxalate and Fe(II) adsorption onto the (010) goethite surface with implications for ligand- and reduction-promoted dissolution. Chemical Geology, 464, 14-22.

Leung, K., and Criscenti, L.J. (2012) Predicting the acidity constant of a goethite hydroxyl group from first principles. Journal of Physics: Condensed Matter, 24, 124105.

Leung, K., and Criscenti, L.J. (2017) Lead and selenite adsorption at water–goethite interfaces from first principles. Journal of Physics: Condensed Matter, 29, 365101.

Lippert, B.G., Hutter, J., and Parrinello, M. (1997) A hybrid gaussian and plane wave density functional scheme. Molecular Physics An International Journal at the Interface Between Chemistry & Physics, 92, 477-487.

Liu, H., Lu, X., Li, M., Zhang, L., Pan, C., Zhang, R., Li, J., and Xiang, W. (2018) Structural incorporation of manganese into goethite and its enhancement of Pb(II) adsorption. Environmental Science & Technology, 52, 4719-4727.

Liu, X., Cheng, J., Lu, X., and Wang, R. (2014a) Surface acidity of quartz: Understanding the crystallographic control. Physical Chemistry Chemical Physics, 16, 26909-26916.

Liu, X., Cheng, J., Sprik, M., Lu, X., and Wang, R. (2013a) Understanding surface acidity of gibbsite with first principles molecular dynamics simulations. Geochimica et Cosmochimica Acta, 120, 487-495.

Liu, X., Cheng, J., Sprik, M., Lu, X., and Wang, R. (2014b) Surface acidity of 2:1-type dioctahedral clay minerals from first principles molecular dynamics

simulations. Geochimica et Cosmochimica Acta, 140, 410-417.

Liu, X., Lu, X., Meijer, E.J., Wang, R., and Zhou, H. (2012a) Atomic-scale structures of interfaces between phyllosilicate edges and water. Geochimica et Cosmochimica Acta, 81, 56-68.

Liu, X., Lu, X., Sprik, M., Cheng, J., Meijer, E.J., and Wang, R. (2013b) Acidity of edge surface sites of montmorillonite and kaolinite. Geochimica et Cosmochimica Acta, 117, 180-190.

Liu, X., Lu, X., Wang, R., Meijer, E.J., Zhou, H., and He, H. (2012b) Atomic scale structures of interfaces between kaolinite edges and water. Geochimica et Cosmochimica Acta, 92, 233-242.

Liu, X., Lu, X., Zhang, Y., Zhang, C., and Wang, R. (2017) Complexation of carboxylate on smectites surfaces. Physical Chemistry Chemical Physics, 19, 18400-18406.

Lutzenkirchen, J. (2002) Surface complexation models of adsorption: A critical survey in the context of experimental data. In Tóth, J. Ed., Adsorption: Theory, modeling, and analysis., pp. 631-710. Marcel Dekker, Inc, 270 Madison Avenue, New York, NY 10016, USA.

Lützenkirchen, J., Boily, J.F., Gunneriusson, L., Lövgren, L., and Sjöberg, S. (2008) Protonation of different goethite surfaces—unified models for NaNO3 and NaCl media. Journal of Colloid and Interface Science, 317, 155-165.

Lützenkirchen, J., Franks, G.V., Plaschke, M., Zimmermann, R., Heberling, F., Abdelmonem, A., Darbha, G.K., Schild, D., Filby, A., Eng, P., Catalano, J.G., Rosenqvist, J., Preocanin, T., Aytug, T., Zhang, D., Gan, Y., and Braunschweig, B. (2018) The surface chemistry of sapphire-c: A literature review and a study on various factors influencing its iep. Advances in Colloid and Interface Science, 251, 1-25.

Majzlan, J., Grevel, K.-D., and Navrotsky, A. (2003) Thermodynamics of Fe oxides: Part ii. Enthalpies of formation and relative stability of goethite (α-FeOOH), lepidocrocite (γ-FeOOH), and maghemite (γ-Fe2O3). American Mineralogist, 88, 855-859.

Mamindy-Pajany, Y., Hurel, C., Marmier, N., and Roméo, M. (2011) Arsenic (V) adsorption from aqueous solution onto goethite, hematite, magnetite and zero-valent iron: Effects of pH, concentration and reversibility. Desalination, 281, 93-99.

Mangold, M., Rolland, L., Costanzo, F., Sprik, M., Sulpizi, M., and Blumberger, J. (2011) Absolute pka values and solvation structure of amino acids from density functional based molecular dynamics simulation. Journal of Chemical Theory and Computation, 7, 1951-1961.

Manning, B.A., Fendorf, S.E., and Goldberg, S. (1998) Surface structures and stability of arsenic(III) on goethite: Spectroscopic evidence for inner-sphere complexes. Environmental Science & Technology, 32, 2383-2388.

Marsac, R., Martin, S., Boily, J.-F., and Hanna, K. (2016) Oxolinic acid binding at goethite and akaganéite surfaces: Experimental study and modeling. Environmental Science & Technology, 50, 660-668.

Martin, G.J., Cutting, R.S., Vaughan, D.J., and Warren, M.C. (2009) Bulk and key surface structures of hematite, magnetite, and goethite: A density functional theory study. American Mineralogist, 94, 1341-1350.

McCarty, D.K., Moore, J.N., and Marcus, W.A. (1998) Mineralogy and trace element association in an acid mine drainage iron oxide precipitate; comparison of selective extractions. Applied Geochemistry, 13, 165-176.

Nie, Z., Finck, N., Heberling, F., Pruessmann, T., Liu, C., and Lützenkirchen, J. (2017) Adsorption of selenium and strontium on goethite: EXAFS study and surface complexation modeling of the ternary systems. Environmental Science & Technology, 51, 3751-3758.

Ona-Nguema, G., Morin, G., Juillot, F., Calas, G., and Brown, G.E. (2005) EXAFS analysis of arsenite adsorption onto two-line ferrihydrite, hematite, goethite, and lepidocrocite. Environmental Science & Technology, 39, 9147-9155.

Ostergren, J.D., Trainor, T.P., Bargar, J.R., Brown, G.E., and Parks, G.A. (2000) Inorganic ligand effects on Pb(II) sorption to goethite (α-FeOOH): I. Carbonate. Journal of Colloid and Interface Science, 225, 466-482.

Park, J.M., Laio, A., Iannuzzi, M., and Parrinello, M. (2006) Dissociation mechanism of acetic acid in water. Journal of the American Chemical Society, 128, 11318-11319.

Perdew, J.P., Burke, K., and Ernzerhof, M. (1997) Generalized gradient approximation made simple. Physical Review Letters, 78, 1396.

Peretyazhko, T., Zachara, J.M., Boily, J.F., Xia, Y., Gassman, P.L., Arey, B.W., and Burgos, W.D. (2009) Mineralogical transformations controlling acid mine drainage chemistry. Chemical Geology, 262, 169-178.

Persson, P., and Axe, K. (2005) Adsorption of oxalate and malonate at the water-goethite interface: Molecular surface speciation from ir spectroscopy. Geochimica et Cosmochimica Acta, 69, 541-552.

Pouvreau, M., Greathouse, J.A., Cygan, R.T., and Kalinichev, A.G. (2017) Structure of hydrated gibbsite and brucite edge surfaces: DFT results and further development of the clayff classical force field with metal–o–h angle bending terms. Journal of Physical Chemistry C, 121, 14757-14771.

Randall, S.R., Sherman, D.M., Ragnarsdottir, K.V., and Collins, C.R. (1999) The mechanism of cadmium surface complexation on iron oxyhydroxide minerals. Geochimica et Cosmochimica Acta, 63, 2971-2987.

Rustad, J.R., and Boily, J.-F. (2010) Density functional calculation of the infrared spectrum of surface hydroxyl groups on goethite (α-FeOOH). American Mineralogist, 95, 414.

Schwertmann, U., and Cornell, R.M. (2000) Iron oxides in the laboratory: Preparation and characterization. John Wiley & Sons.

Schwertmann, U., and Taylor, R.M. (1989) Iron oxides. Minerals in soil environments, 1, 379-438.

Spadini, L., Manceau, A., Schindler, P.W., and Charlet, L. (1994) Structure and stability of Cd2+ surface complexes on ferric oxides: 1. Results from EXAFS spectroscopy. Journal of Colloid and Interface Science, 168, 73-86.

Sparks, D.L. (2003) Environmental soil chemistry. Academic press.

Sulpizi, M., Gaigeot, M.-P., and Sprik, M. (2012) The silica–water interface: How the silanols determine the surface acidity and modulate the water properties. Journal of Chemical Theory and Computation, 8, 1037-1047.

Sulpizi, M., and Sprik, M. (2008) Acidity constants from vertical energy gaps: Density functional theory based molecular dynamics implementation. Physical Chemistry Chemical Physics, 10, 5238-5249.

Sulpizi, M., and Sprik, M. (2010) Acidity constants from DFT-based molecular dynamics simulations. Journal of Physics: Condensed Matter, 22, 284116.

Tournassat, C., Davis, J.A., Chiaberge, C., Grangeon, S., and Bourg, I.C. (2016) Modeling the acid–base properties of montmorillonite edge surfaces. Environmental Science & Technology, 50, 13436-13445.

Tournassat, C., Tinnacher, R.M., Grangeon, S., and Davis, J.A. (2018) Modeling uranium(VI) adsorption onto montmorillonite under varying carbonate concentrations: A surface complexation model accounting for the spillover effect on surface potential. Geochimica et Cosmochimica Acta, 220, 291-308.

van der Zee, C., Roberts, D.R., Rancourt, D.G., and Slomp, C.P. (2003) Nanogoethite is the dominant reactive oxyhydroxide phase in lake and marine sediments. Geology, 31, 993-996.

VandeVondele, J., and Hutter, J. (2007) Gaussian basis sets for accurate calculations on molecular systems in gas and condensed phases. The Journal of Chemical Physics, 127, 114105.

VandeVondele, J., Krack, M., Mohamed, F., Parrinello, M., Chassaing, T., and Hutter, J. (2005) Quickstep: Fast and accurate density functional calculations using a mixed gaussian and plane waves approach. Computer Physics Communications, 167, 103-128.

VandeVondele, J., Mohamed, F., Krack, M., Hutter, J., Sprik, M., and Parrinello, M. (2004) The influence of temperature and density functional models in ab initio molecular dynamics simulation of liquid water. The Journal of Chemical Physics, 122, 014515.

Venema, P., Hiemstra, T., and van Riemsdijk, W.H. (1997) Interaction of cadmium with phosphate on goethite. Journal of Colloid and Interface Science, 192, 94-103.

Venema, P., Hiemstra, T., Weidler, P.G., and van Riemsdijk, W.H. (1998) Intrinsic proton affinity of reactive surface groups of metal (hydr)oxides: Application to iron (hydr)oxides. Journal of Colloid and Interface Science, 198, 282-295.

von Rudorff, G.F., Jakobsen, R., Rosso, K.M., and Blumberger, J. (2016) Hematite(001)-liquid water interface from hybrid density functional-based molecular dynamics. Journal of Physics: Condensed Matter, 28, 394001.

Watts, H.D., Tribe, L., and Kubicki, J.D. (2014) Arsenic adsorption onto minerals: Connecting experimental observations with density functional theory calculations. Minerals, 4, 208-240.

Yan, W., and Jing, C. (2018) Molecular insights into glyphosate adsorption to goethite gained from ATR-FTIR, two-dimensional correlation spectroscopy, and DFT study. Environmental Science & Technology, 52, 1946-1953.

Yang, Y., Wang, S., Xu, Y., Zheng, B., and Liu, J. (2016) Molecular-scale study of aspartate adsorption on goethite and competition with phosphate. Environmental Science & Technology, 50, 2938-2945.

Zhang, C., Liu, X., Lu, X., He, M., Jan Meijer, E., and Wang, R. (2017) Surface complexation of heavy metal cations on clay edges: Insights from first principles molecular dynamics simulation of Ni(II). Geochimica et Cosmochimica Acta, 203, 54-68.

Zhang, C., Liu, X., Lu, X., Meijer, E.J., Wang, K., He, M., and Wang, R. (2016) Cadmium(II) complexes adsorbed on clay edge surfaces: Insight from first principles molecular dynamics simulation. Clays and Clay Minerals, 64, 337-347.

Zhang, C., Liu, X., Tinnacher, R.M., and Tournassat, C. (2018) Mechanistic understanding of uranyl ion complexation on montmorillonite edges: A combined first-principles molecular dynamics–surface complexation modeling approach. Environmental Science and Technology, 52, 8501-8509.

Zhang, Y., Liu, X., Zhang, C., and Lu, X. (2020) A combined first principles and classical molecular dynamics study of clay-soil organic matters (soms) interactions. Geochimica et Cosmochimica Acta, 291, 110-125.

Endnote:

[1]Supplemental Material.

This is the peer-reviewed, final accepted version for American Mineralogist, published by the Mineralogical Society of America.
The published version is subject to change. Cite as Authors (Year) Title. American Mineralogist, in press.
DOI: https://doi.org/10.2138/am-2021-7835. http://www.minsocam.org/

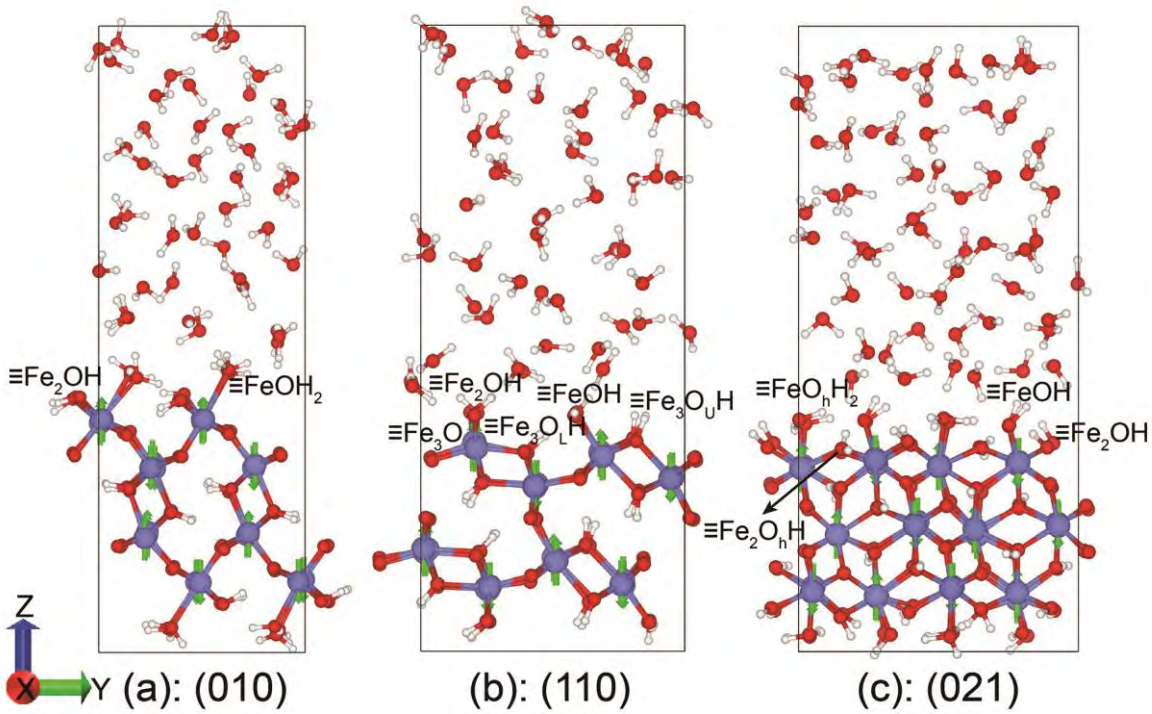

FIGURE 1. The surface models used in the study. O = red, H = white, Fe = blue-violet. Green arrows indicate the electron spin orientations.

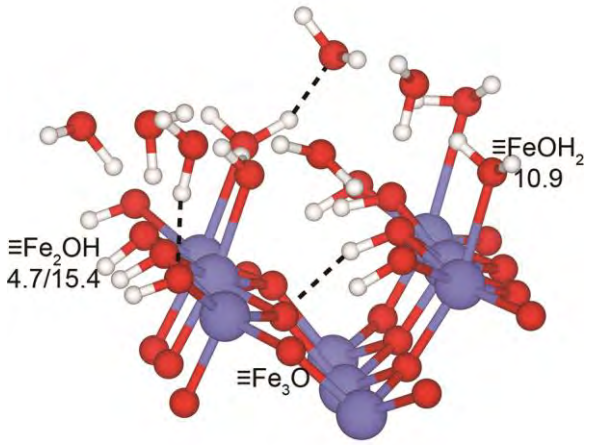

643

644 **FIGURE 2.** Snapshot of the (010) surface. Atoms are color-coded by element as

645 described in Figure 1. Only the water molecules that hydrogen-bonded with surface

646 groups are depicted and the others are removed for clarity.

647

This is the peer-reviewed, final accepted version for American Mineralogist, published by the Mineralogical Society of America.
The published version is subject to change. Cite as Authors (Year) Title. American Mineralogist, in press.
DOI: https://doi.org/10.2138/am-2021-7835. http://www.minsocam.org/

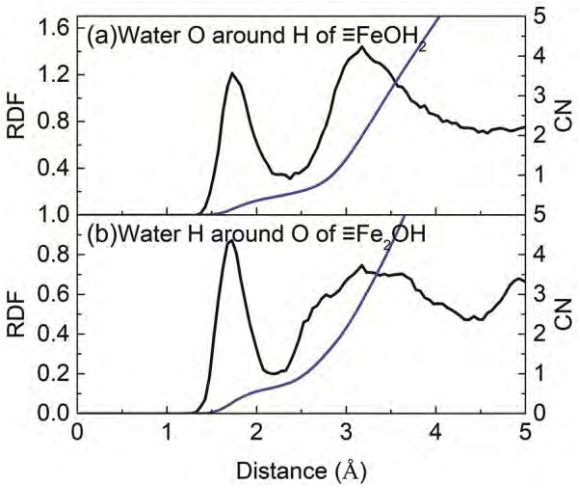

FIGURE 3. Radial distribution function (RDF) and coordination number (CN) for (**a**) water O around H of ≡$FeOH_2$ and (**b**) water H around O of ≡Fe_2OH on (010) surface.

This is the peer-reviewed, final accepted version for American Mineralogist, published by the Mineralogical Society of America.
The published version is subject to change. Cite as Authors (Year) Title. American Mineralogist, in press.
DOI: https://doi.org/10.2138/am-2021-7835. http://www.minsocam.org/

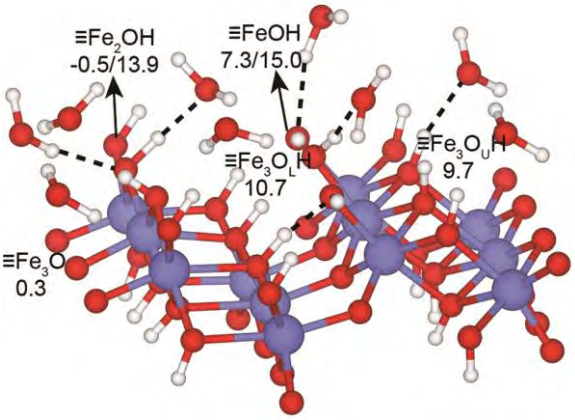

FIGURE 4. Snapshot of the (110) surface. Atoms are color-coded by element as described in Figure 1. Only the water molecules that hydrogen-bonded with surface groups are depicted and the others are removed for clarity.

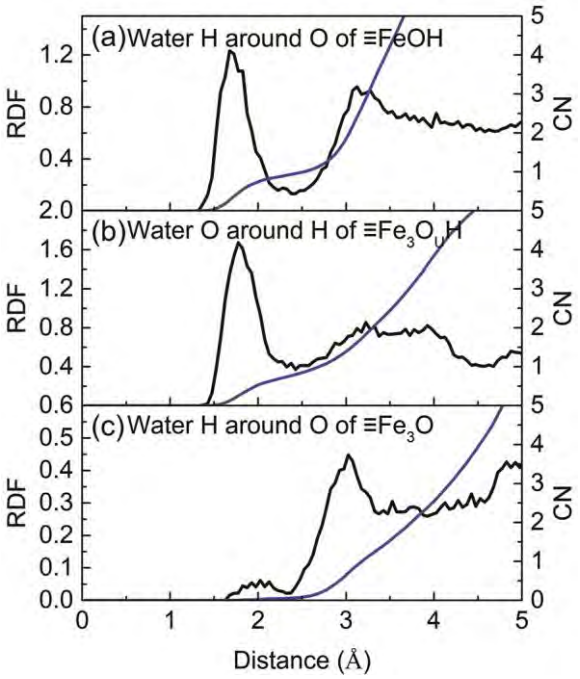

FIGURE 5. RDF and CN for (**a**) water H around O of ≡FeOH, (**b**) water O around H of ≡Fe_3O_UH, and (**c**) water H around O of ≡Fe_3O on (110) surface.

This is the peer-reviewed, final accepted version for American Mineralogist, published by the Mineralogical Society of America.
The published version is subject to change. Cite as Authors (Year) Title. American Mineralogist, in press.
DOI: https://doi.org/10.2138/am-2021-7835. http://www.minsocam.org/

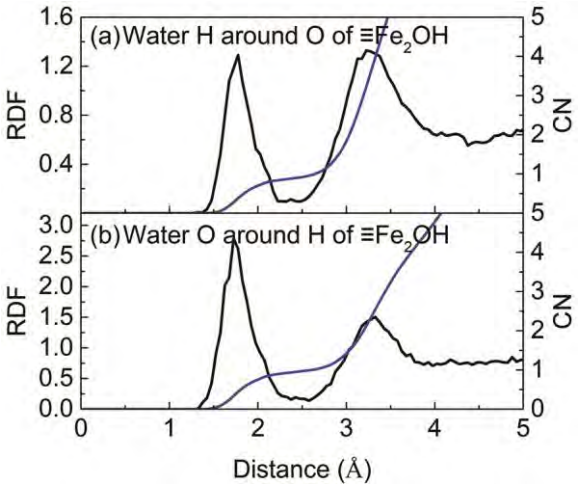

662

663 **FIGURE 6.** RDF and CN for (**a**) water H around O of ≡Fe_2OH and (**b**) water O

664 around H of ≡Fe_2OH on (110) surface.

665

This is the peer-reviewed, final accepted version for American Mineralogist, published by the Mineralogical Society of America.
The published version is subject to change. Cite as Authors (Year) Title. American Mineralogist, in press.
DOI: https://doi.org/10.2138/am-2021-7835. http://www.minsocam.org/

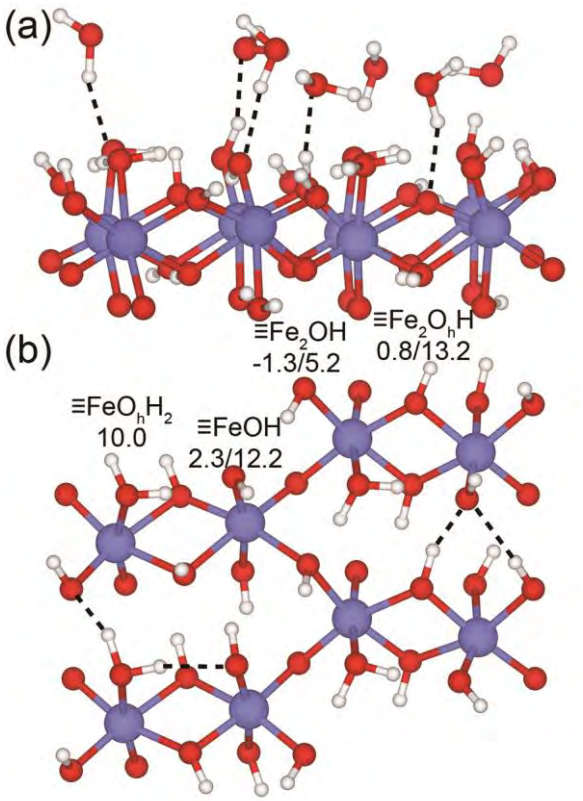

666

667 **FIGURE 7.** Snapshot of the (021) surface. (**a**) side view showing the hydrogen
668 bonds between surface groups and water molecules; (**b**) top view showing the
669 hydrogen bonds between surface groups. Atoms are color-coded by element as
670 described in Figure 1. Only the water molecules that hydrogen-bonded with surface
671 groups are depicted and the others are removed for clarity.

672

This is the peer-reviewed, final accepted version for American Mineralogist, published by the Mineralogical Society of America.
The published version is subject to change. Cite as Authors (Year) Title. American Mineralogist, in press.
DOI: https://doi.org/10.2138/am-2021-7835. http://www.minsocam.org/

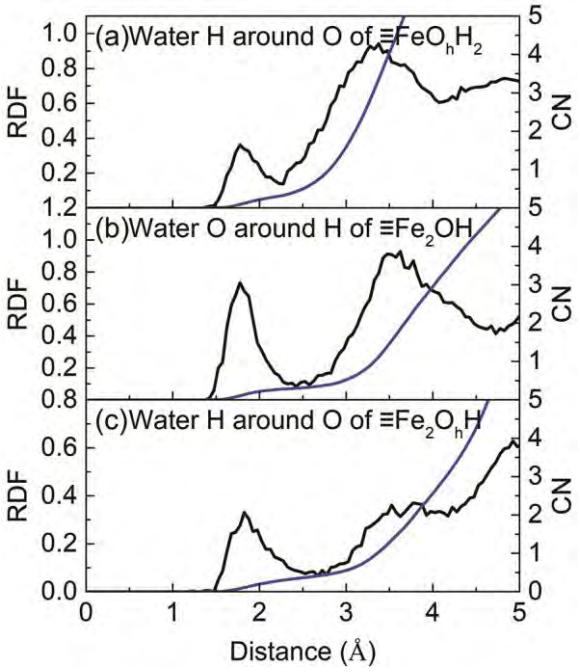

673

674 **FIGURE 8.** RDF and CN for (**a**) water H around O of ≡FeO_hH_2, (**b**) water O

675 around H of ≡Fe_2OH, and (**c**) water H around O of ≡Fe_2O_hH on (021) surface.

676

This is the peer-reviewed, final accepted version for American Mineralogist, published by the Mineralogical Society of America.
The published version is subject to change. Cite as Authors (Year) Title. American Mineralogist, in press.
DOI: https://doi.org/10.2138/am-2021-7835. http://www.minsocam.org/

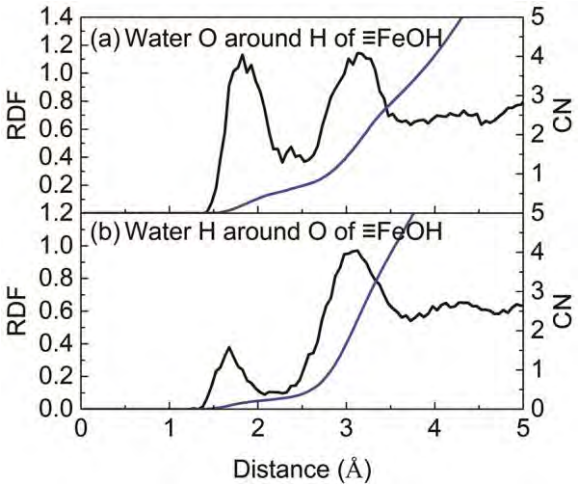

677

678 **FIGURE 9.** RDF and CN for (**a**) water O around H of ≡FeOH and (**b**) water H

679 around O of ≡FeOH on (021) surface.

680

681 **TABLE 1.** Calculated pKa values of groups on (010) surface in comparison with

682 MUSIC results

Groups	This study	MUSIC[a]
$\equiv FeOH_2$	10.9±1.8	
$\equiv Fe_2OH_2/\equiv Fe_2OH$	4.7±0.8/15.4±0.7	4.3/-

[a](Boily, 2012).

683

684

685 **TABLE 2.** Calculated pKa values of surface groups on (110) surface in comparison

686 with literature results

Groups	This study	MUSIC[a]			FPMD[b]
		I	II	III	
$\equiv FeOH_2/\equiv FeOH$	7.3±0.5/15.0±0.7	11.7/23.6	7.7/19.6	3.7/15.6	7.0/-
$\equiv Fe_2OH_2/\equiv Fe_2OH$	-0.5±1.3/13.9±0.7	0.4/12.3			
$\equiv Fe_3O_LH$	10.7±0.5	11.7			
$\equiv Fe_3O_UH$	9.7±0.7	11.7			
$\equiv Fe_3OH$	0.3±0.8	-0.2			

[a](Venema et al., 1998; Gaboriaud and Ehrhardt, 2003): I, II, and III mean that 1, 2, and 3 hydrogen bonds are presumed between surface groups and water, respectively. [b](Leung and Criscenti, 2012).

687

688

689 **TABLE 3.** Calculated pKa values of surface groups on (021) surface in comparison

690 with MUSIC results

Groups	This study	MUSIC[a]
$\equiv FeO_hH_2$	10.0±1.5	11.9
$\equiv FeOH_2/\equiv FeOH$	2.3±1.2/12.2±1.7	8.1/20.0
$\equiv Fe_2OH_2/\equiv Fe_2OH$	-1.3±2.0/5.2±1.3	0.0/11.9
$\equiv Fe_2O_hH_2/\equiv Fe_2O_hH$	0.8±1.7/13.2±1.0	7.7/19.6

[a](Venema et al., 1998).

691

692

693 **TABLE 4.** Calculated pKa values of surface groups and PZC of individual surfaces

Surface	Groups	pKa	PZC
(010)	$\equiv FeOH_2$	10.9	7.8
	$\equiv Fe_2OH_2/\equiv Fe_2OH$	4.7/15.4	
(110)	$\equiv FeOH_2/\equiv FeOH$	7.3/15.0	8.5
	$\equiv Fe_2OH_2/\equiv Fe_2OH$	-0.5/13.9	
	$\equiv Fe_3O_LH$	10.7	
	$\equiv Fe_3O_UH$	9.7	
	$\equiv Fe_3O$	0.3	
(021)	$\equiv FeO_hH_2$	10.0	3.8
	$\equiv FeOH_2/\equiv FeOH$	2.3/12.2	
	$\equiv Fe_2OH_2/\equiv Fe_2OH$	-1.3/5.2	
	$\equiv Fe_2O_hH_2/\equiv Fe_2O_hH$	0.8/13.2	

694

695

696